NUMERICAL MODELING OF HYPOLIMNETIC OXYGENATION BY ELECTROLYSIS OF WATER

by

Nenad M. JAĆIMOVIĆ[a*], Takashi HOSODA[b], Park HO-DONG[c], and Marko V. IVETIĆ[a]

[a] Department of Hydraulic and Environmental Engineering, Faculty of Civil Engineering, University of Belgrade, Belgrade, Serbia

[b] Kyoto University, Kyoto, Japan

[c] Shinshu University, Matsumoto, Japan

Original scientific paper
DOI: 10.2298/TSCI????

The paper presents a novel method for hypolimnetic oxygenation by electrolysis of water. The performance of the method is investigated by the laboratory and the field experiment. The laboratory experiment is conducted in a 90L vessel, while the field experiment is conducted at the lake Biwa in Japan. In order to provide a better insight into involved processes, a numerical model for simulation of bubble flow is developed with consideration of gas compressibility and oxygen dissolution. The model simultaneously solves three-dimensional volume averaged two-fluid governing equations. Developed model is firstly verified by simulation of bubble flow experiments, reported in the literature, where good qualitative agreement between measured and simulated results is observed. In the second part, the model is applied for simulation of conducted water electrolysis experiments. The model reproduced the observed oxygen concentration dynamics reasonably well.

Key words: *eutrophication, electrolysis, oxygenation, numerical model*

Introduction

Eutrofication is a natural process of primary production increase in lakes, which may lead to severe deterioration of water quality [1-3]. These processes are significantly affected by thermal stratification [4-6], due to formation of density and temperature structure consisting of relatively homogeneous surface water layer which is separated from the deep hypolimnion zone by a layer with the strong temperature gradient, referenced as metalimnion. The metalimnion has effective role of barrier that prevents exchange of dissolved oxygen from the surface layer. Due to excessive release of nutrients by human activities, this process is significantly accelerated and, in extreme cases, to anoxic conditions [7-9].

Low levels of dissolved oxygen (DO) have extremely negative consequences on ecological status, as well as on drinking water treatment process in the case of water supply

* Corresponding author; e-mail: njacimovic@hikom.grf.bg.ac.rs

reservoirs [10]. This includes production of hydrogen sulfide and ammonia, and may lead to reactivation of heavy metals and nutrients from the sediment [11, 12].

One of available lake restoration strategies is hypolimnetic oxygenation, with idea to replenish the dissolved oxygen (DO) by aeration, while preserving the thermal stratification [13-19]. Gafsi et al. [16] concluded that aeration by oxygen has significant advantages in comparison with aeration by air. In this case, very efficient oxygen transfer can be achieved.

In this paper we propose a novel technology, which includes electrolysis of water at the lake bottom, with oxygen dissolution and possible hydrogen harvesting for further energy purposes. For simulation of the processes associated with the proposed technology, a numerical model for bubble flow simulation is developed, with the consideration of gas compressibility and oxygen dissolution. The model has the aim to provide a better insight into the processes related with oxygen bubble production and its dissolution in the water. The model solves three dimensional volume-averaged, two-fluid governing equations. The developed model is verified by simulation of bubble flow experiments, previously reported in the literature. Different flow configurations are tested: in which quasi-steady state is achieved, and where steady conditions cannot develop. In the second part, the model is applied for simulation of the conditions achieved in the electrolysis laboratory and field experiments conducted in this study. This is a new approach aimed at providing the oxygen directly from the water.

The paper is organized as follows. In the first section the description of the experimental part of the study is given. Then, we present the numerical model developed in this study with the non-linear turbulence closure equations. We finally compare and discuss numerical results and experimental data.

Experimental study

The experimental study of electrolysis effects on DO rehabilitation has been performed in the laboratory (at the Shinshu University) and in the field conditions. The laboratory setup consisted of the 90 L transparent vessel, with 56.6 cm water depth. The electrolysis apparatus (7.0 cm in height) consists of seven pairs of platinum plates (20 × 7 cm), placed at the middle of the vessel bottom. Direct current of 2.3 A is applied, and transient DO concentrations are measured at different levels, in the center of horizontal plane section. Control levels are at 25 cm, 35 cm, and 45 cm from the vessel bottom.

The gas phase (hydrogen and oxygen) is uniformly produced at the 7.5 cm above the bottom, at the horizontal area 20 × 10 cm. The volume of produced oxygen by electrolysis is calculated from the Faraday's law:

$$\frac{24.8L/mol \cdot 2.3A}{4 \cdot 96485As/mol} = 0.148 \cdot 10^{-3} L/s$$

which, expressed per minute at 1.05 atm pressure, gives 8.46×10^{-3} L/min. The volume of produced hydrogen may be considered as double of this value.

After imposing the current through the electrolysis setup, a stream of hydrogen and oxygen bubbles, due to buoyancy, starts to flow upward. This stream entrains the surrounding water phase, which causes circulation of the water (Figure 1). The electrolysis produced the significant increase of DO concentrations, while the induced water circulation enhanced its dispersion. As a result, relatively uniform DO distribution is observed within the vessel, reaching the DO limit in nearly 8 hours (from initial 2 mg/L to final 13.5 mg/L).

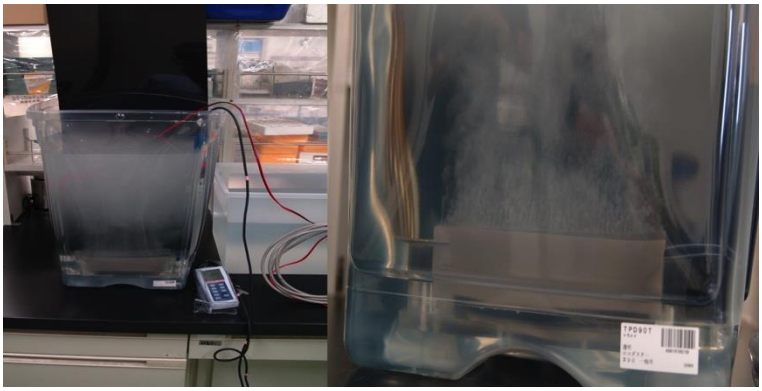

Figure 1. Experimental setup for electrolysis experiment in the laboratory

The field experiment has been conducted at the lake Biwa in Japan. Installation consisted of the plexiglas box with dimensions 130 × 77 × 100 cm. The box bottom was open and the top of the box was partially closed with the two 17 × 3 cm openings at the top cover. Three electrolysis devices were placed at the box bottom, in the middle of the box length (Figure 2). The purpose of the box was to attenuate lateral currents and to accelerate the experiment by reducing the volume of influenced water.

The water column was relatively homogeneous regarding the temperature distribution (14.5 °C). Other water quality parameters were observed as follows: pH = 5.8, Cond = 18.5 mS/m, Turb = 6.1 NTU, TDS = 0.12 g/L and oxidation reduction potential ORP = -89 mV. During the experiment, the hydrogen bubbles were captured with the plastic covers and removed from the box by pipes.

The water depth at the experiment site was 10 m. The DO concentration was measured 38 cm below the box cover (Horiba W-23XD monitoring system), at the middle of the smaller vertical wall, 2.5 cm from the wall.

The direct current of 7.71, 7.91, and 8.05 A was imposed on three devices respectively. Taking into account water pressure at 10 m of water column, calculated total oxygen production was 0.0412 L/min. After imposing the current, the DO concentration was continually observed. The recorded increase of DO concentration was approximately linear with the time. After 87 minutes, the DO concentration increased from initial 0.4 mg/L to 6.4 mg/L.

Outline of the numerical model

Several approaches has been proposed in the literature for bubble plumes modeling. The most often applied are models based on one-dimensional (1D), transversally integrated equations and self-similar solutions [17-21]. They provide a simple and robust tool for estimation of mechanical efficiency (mixing rate) and oxygen transfer, if considered. Naturally, such models cannot account for possible crossflow effects and oxygen transfer by low level aeration. Bernard et al. [22] proposed relatively simple three-dimensional (3D) single-phase model with the implementation of turbulence effects. In their model, authors idealized the bubble plume as a cylindrical volume within which all bubbles remain and rise vertically by the assumed slip velocity. As authors pointed out, the model is not applicable in the stratified environment, due to uniform bubble column approximation.

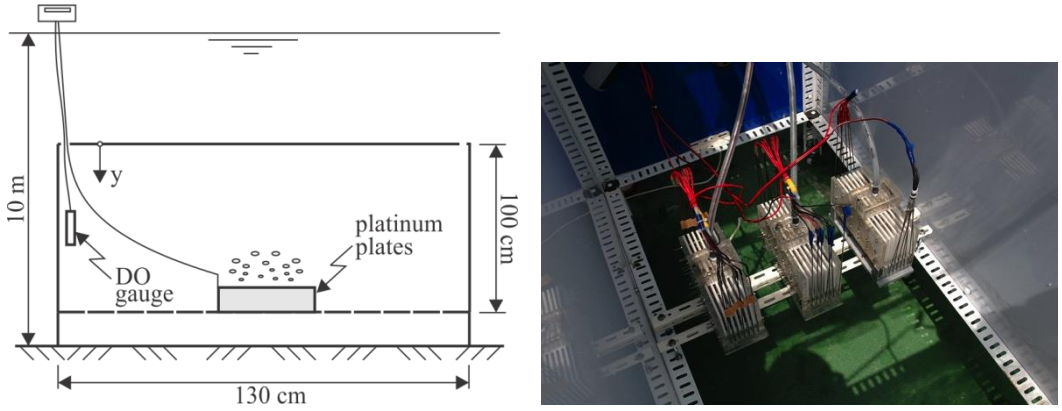

Figure 2. Left: Schematic representation of the field experiment; Right: three electrolysis devices installed at the box bottom.

Two phase models [23-26] provide a better insight into the effectiveness of the applied aeration technology. Here, several approaches are possible for coupling the gas and water phases: (1) Eulerian-Eulerian (EE), (2) Eulerian-Lagrangian (EL), where gas bubbles are treated as Lagrangian markers, and (3) Interface tracking method, in which a numerical method has to be applied for tracking of the boundary between two phases. The well known Volume of Fluid (VOF) [27] method may be considered as a representative for this approach.

In the pioneering work of multidimensional, two phase modeling of bubble plumes, Sokolichin and Eigenberger [23] considered EE and EL methods, and concluded that EL approach potentially have advantages in large scale geometry. However, a detailed computational comparison [28] revealed that EE based models provide similar results as EL models in terms of accuracy of average flow quantities.

Fraga et al. [26] proposed recently an advanced large-eddy simulation (LES) - based EL model for simulation of bubble plume dynamics which is applied to the simulation of laboratory experiments. They concluded that bubble-induced turbulence generation may play an important role and should be further investigated. However, the real scale application of the model, e.g. for hypolimnetic aeration of stratified lakes, is not discussed.

In this study a two-phase EE model is proposed, based on the volume-averaged Raynolds-averaged Navier-Stokes equations (VARANS). Considering compressibility of the gas phase, and the mass transfer between the phases, continuity equations for the gas and the water phase can be obtained by the volume averaging (e.g. [29]):

$$\frac{\partial\left(\rho_g \alpha_g\right)}{\partial t} + \frac{\partial\left(\rho_g \alpha_g V_{gj}\right)}{\partial x_j} = -G_{gw} \tag{1}$$

$$\frac{\partial \alpha_w}{\partial t} + \frac{\partial\left(\alpha_w V_{wj}\right)}{\partial x_j} = \frac{G_{gw}}{\rho_w} \tag{2}$$

$$\alpha_g + \alpha_w = 1 \tag{3}$$

where subscripts g and w denote gas and water phase, respectively, x_j is the Cartesian coordinate, t is the time, ρ is the phase density, α is the phase content, V_j is the component of velocity vector and G_{gw} is the mass transfer between two phases, per unit time and volume.

It is assumed that density of the gas phase comply with the ideal gas law:

$$\rho_g = \frac{p_g m_g}{RT} \tag{4}$$

where p_g is the gas pressure, m_g is the gas molar mass, T is the absolute temperature, and R is the gas constant (= 0.08206 L·atm·K^{-1}·mol^{-1}).

Dissolution of oxygen into the water phase is modeled as a first-order process, proposed by Wuest [18]:

$$G_{gw} = K_{gw} A\left(H p_g - DO\right) \tag{5}$$

where K_{gw} is the mass transfer coefficient, A is the gas-water surface area, H is the dimensional Henry's constant, and DO is the dissolved oxygen.

During the buoyancy-forced flow of bubbles, their size is changing due to pressure change, as well as due to dissolution. In order to model this change, a number of bubbles is updated at each time step by solution of the following advection equation:

$$\frac{\partial N_b}{\partial t} + \frac{\partial\left(N_b V_{gj}\right)}{\partial x_j} = 0 \tag{6}$$

where N_b is the number of bubbles per unit volume. Bubble diameter is calculated from the gas content and number of bubbles, and it is utilized to calculate the drag force and gas-water surface area through which the oxygen mass transfer occurs.

Volume averaged momentum equations can be formulated as:

$$\frac{\partial\left(\rho_g \alpha_g V_{gi}\right)}{\partial t} + \frac{\partial\left(\rho_g \alpha_g V_{gi} V_{gj}\right)}{\partial x_j} = -\alpha_g \frac{\partial p_g}{\partial x_i} - \rho_g \alpha_g g_i - F_{gw} \tag{7}$$

$$\frac{\partial\left(\alpha_w V_{wi}\right)}{\partial t} + \frac{\partial\left(\alpha_w V_{wi} V_{wj}\right)}{\partial x_j} = -\frac{\alpha_w}{\rho_w}\frac{\partial p_w}{\partial x_i} - \alpha_w g_i + \frac{1}{\rho_w}\frac{\partial\left(\alpha_w \tau_{ij}\right)}{\partial x_j} + \frac{1}{\rho_w} F_{gw} \tag{8}$$

in which g_i is the component of gravitational acceleration, τ_{ij} is the shear stress, including viscous and turbulent effects, and F_{gw} is the momentum interaction term [29]. The latter is modeled considering three components:

$$F_{gw} = F_d + F_{am} + F_l \tag{9}$$

where F_d is the drag force, F_{am} is the added mass force, and F_l is the lift force. These forces are calculated as follows:

$$F_d = \frac{1}{2} C_d \rho_w \pi \frac{d_b^2}{4} \left|V_g - V_w\right|\left(V_g - V_w\right) \tag{10}$$

$$F_{am} = C_v \rho_w \alpha_g \left(\frac{DV_g}{Dt} - \frac{DV_w}{Dt} \right) \tag{11}$$

$$F_l = C_v \rho_w \alpha_w (V_g - V_w) \times \left(\nabla \times V_g \right) \tag{12}$$

where C_d is the drag coefficient, d_b is the bubble diameter, C_v is the coefficient, and ∇ is the divergence operator. The drag coefficient is calculated as a function of Raynolds and Eotwos numbers [30]:

$$C_d = \max\left[\frac{24}{\mathrm{Re}} \left(1 + 0.15 \mathrm{Re}^{0.687}\right), \frac{8}{3}, \frac{Eo}{Eo+4} \right] \tag{13}$$

Presented governing equations are discretized by finite volumes with staggered arrangement of flow variables. Pressure and velocity fields, at each time step, are calculated using the Highly Simplified Marker and Cell (HSMAC) method [31], with application of Adams-Bashforth scheme for time integration of convective and viscous terms in momentum equations. For solution of continuity equations (1), (2), as well as equation (6), a higher order approach is utilized by linear interpolation of variables and application of TVD limiters [32], in order to prevent oscillations and to minimize numerical dispersion effects.

Sokolichin and Eigenberger [33] analyzed applicability of the standard *k*-ε turbulence model for simulation of bubble plumes. The simulation of experiments conducted in laboratory vessels revealed very good qualitative and acceptable quantitative predictions; in spite the fact that bubble induced turbulence was not considered. They emphasized the sensitivity of results to the approximation of the convective terms in the model formulation. Buscaglia, et al. [25] argued that the two-phase, bubble induced turbulence closure is still far from the clear resolution, although some authors have proposed corrections to the *k*-ε equations to account this effect. Recent studies reveal that bubbles induce significant turbulence of anisotropic nature, even at low Reynolds numbers [34].

In this study, we applied a non-linear *k*-ε turbulence model [35]. No corrections for bubble induced turbulence are included:

$$-\overline{u_i' u_j'} = \nu_t S_{ij} - \frac{2}{3} k \delta_{ij} - \frac{k}{\varepsilon} \nu_t \sum_{\beta=1}^{3} C_\beta \left(S_{\beta ij} - \frac{1}{3} S_{\beta \alpha \alpha} \delta_{ij} \right) \tag{14}$$

$$\nu_t = C_\mu \frac{k^2}{\varepsilon} \tag{15}$$

$$\frac{\partial \alpha_w k}{\partial t} + \frac{\partial \alpha_w k u_j}{\partial x_j} = -\alpha_w \overline{u_i' u_j'} \frac{\partial u_i}{\partial x_j} - \alpha_w \varepsilon + \frac{\partial}{\partial x_j} \left[\alpha_w \left(\frac{\nu_t}{\sigma_k} + \nu \right) \frac{\partial k}{\partial x_j} \right] \tag{16}$$

$$\frac{\partial \alpha_w \varepsilon}{\partial t} + \frac{\partial \alpha_w \varepsilon u_j}{\partial x_j} = -\alpha_w C_{\varepsilon 1} \frac{\varepsilon}{k} \overline{u_i' u_j'} \frac{\partial u_i}{\partial x_j} - \alpha_w C_{\varepsilon 2} \frac{\varepsilon^2}{k} + \frac{\partial}{\partial x_j} \left[\alpha_w \left(\frac{\nu_t}{\sigma_\varepsilon} + \nu \right) \frac{\partial \varepsilon}{\partial x_j} \right] \tag{17}$$

$$S_{ij} = \frac{\partial u_i}{\partial x_j} + \frac{\partial u_j}{\partial x_i} \tag{18a}$$

$$S_{1ij} = \frac{\partial u_i}{\partial x_r}\frac{\partial u_j}{\partial x_r}, \quad S_{2ij} = \frac{1}{2}\left(\frac{\partial u_r}{\partial x_i}\frac{\partial u_j}{\partial x_r} + \frac{\partial u_r}{\partial x_j}\frac{\partial u_i}{\partial x_r}\right), \quad S_{3ij} = \frac{\partial u_r}{\partial x_i}\frac{\partial u_r}{\partial x_j} \tag{18b}$$

where $-\overline{u_i'u_j'}$ = Reynolds stress, k = turbulent kinetic energy, ε = dissipation rate, and ν_t = eddy viscosity coefficient. The model coefficient C_μ is a function of strain and rotation parameters, as described with model parameters in the reference [35].

For simulation of DO dissolution/transport in the water, an additional DO transport equation has to be solved:

$$\frac{\partial(\alpha_w DO)}{\partial t} + \frac{\partial}{\partial x_j}\left(\alpha_w DOV_{wj}\right) = \frac{\partial}{\partial x_j}\left(\alpha_w D_w \frac{\partial DO}{\partial x_j}\right) + G_{gw} \tag{19}$$

where D_w is the effective dispersion coefficient.

Electrolysis produces hydrogen and oxygen in the 2:1 molar ratio. In the laboratory experiment simulated in this study, hydrogen is not removed after bubble-up at the cathode, and therefore, it affects flow and distribution of oxygen bubbles, as well as DO distribution. In order to track hydrogen and oxygen number of bubbles, equation (6) is solved separately. Since the size of hydrogen and oxygen bubbles is not the same, for calculation of the momentum interaction term in equations (7) and (8), the volume-weighted representative diameter is calculated from available volumetric contents:

$$\overline{d_b} = \frac{d_{O2}\alpha_{O2} + d_H\alpha_H}{\alpha_g} \tag{20}$$

where $\overline{d_b}$ is the representative bubble diameter, α_{O2} and α_H are volumetric contents of oxygen and hydrogen, respectively, d_{O2} is the oxygen bubble diameter and d_H is the bubble diameter of hydrogen.

Model validation

Simulation of air flow/distribution during its constant rate injection

As an addition to already reported simulation results [36], the model performance regarding flow and air distribution is validated by application to another reported experiments [37], conducted in a flat bubble column 50 cm wide, 200 cm high and 8 cm thick. Air sparger was centered at the bottom, through which different air injection flow rates were applied in different experiments. The water level in the column is also varied for different experiments. Bubble plumes were visually observed through transparent column walls. In addition, a Laser Doppler Anemometer was used to measure velocity magnitudes of the water phase in the mid-plane of column depth (4cm from the walls), at regular grid points (10 cm or 20 cm apart).

In the first case, the experiment with 100 cm water depth is simulated. Air flow rate is 1.0 L/min. Simulation domain is discretized by 50 × 4 × 25 calculation cells, and simulation time step of 0.001 sec is adopted. The air bubble diameter is taken as uniform in the plume, 4 mm as average observed during experiments [37].

In this case, it is reported that no steady flow conditions could be established. Periodic flow with two staggered rows of vortices moving downward was observed, due to which the bubble plume also periodically bends. This behavior is reproduced well by numerical model. Figure 3 shows the bubble at one time section. Left figures show observed bubble plume, while middle and right figures show calculated air distribution and velocity vectors of the water phase. The model reproduced the dynamics of bubble plume bending very well.

In the second case, the experiment with water level at 50 cm from the bottom is chosen. Air flow rate is 2.0 L/min. Simulation domain is discretized by $25 \times 4 \times 25$ cells, and simulation time step of 0.001 sec is adopted again. Depending on the start-up conditions, the authors reported formation of a single vortex, near the center of the flow domain, in the clockwise or counter clockwise direction. Quantitative comparison of simulated and measured velocities for quasi-steady conditions is shown in fig. 4. Good overall agreement of the developed flow field can be observed. The flow is characterized by a single, almost centrally placed, vortex with near stagnant water in the top and bottom right corners.

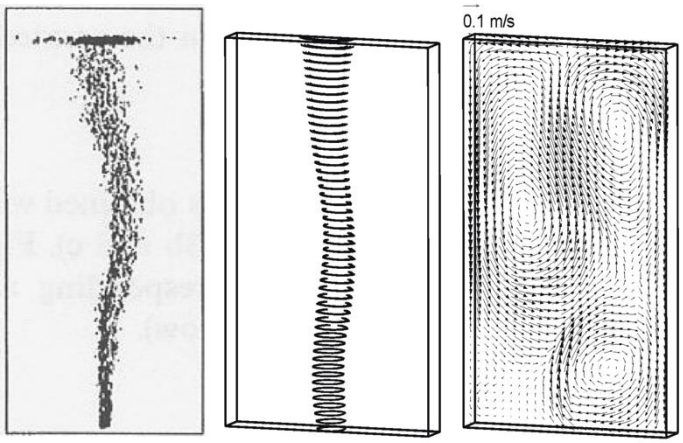

Figure 3. Comparison of observed and simulated bubble plumes for two time sections at 1L/min air flow rate.

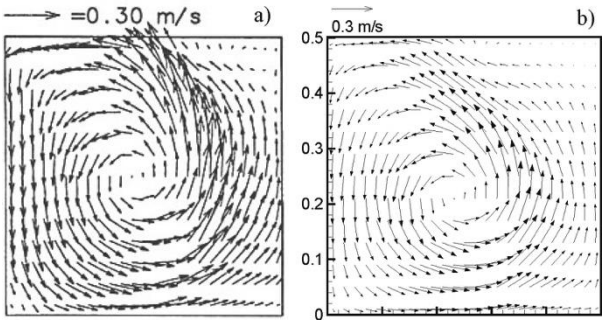

Figure 4. Comparison of observed and simulated velocity mid-profile for steady conditions at 2 L/min air flow rate: a) reported water phase velocities (after Borchers et al. 1999), b) simulation results.

Simulation of the laboratory electrolysis experiment

For the numerical simulation of the laboratory experiment conducted in this study, the domain is discretized by rectangular cells with 5 × 5 cm grid size in the horizontal plane, and varying size in vertical direction: from 5cm at the bottom, to 1.2 cm at the water surface. The total volume of water is 90.6 L.

The starting diameter of the gas bubbles is assumed as 0.1mm. Consequently, mass transfer coefficient in equation (5) is taken as 1.0×10^{-4} m/s. This coefficient depends on bubble size, however, in this study it is taken as a constant, assuming that bubble size does not change significantly.

Prior the electrolysis, measured DO concentrations were 0 mg/L at 25 cm, 0.318 mg/L at 35 cm, and 0.746 mg/L at 45 cm from the bottom. After the start of electrolysis, recorded values showed that DO increased very fast at 35 cm and 45 cm levels. After 2 minutes, measured DO concentration was 2.96 mg/L at 35 cm, and 3.78 mg/L at 45 cm. Such a large increase of DO in a short period of time, after start of electrolysis, could not be resolved by model described by equation (5). Therefore, in the simulation described here, a uniform initial DO concentration of 2.0 mg/L was applied. This is the reason for discrepancy between measured and calculated DO in the early stage of experiment. The agreement in the later stage is good, as shown in fig. 5.

Experimental results indicate and numerical simulation confirmed intensive mixing due to induced water circulation, resulting in uniform distribution of the DO. That is the reason the Figure 5 contains only one line representing the simulation results.

The size of released bubbles certainly has the influence on the dynamics of the DO increase. This is not a linear correlation, since the mass transfer coefficient is also function of the bubble diameter. The effect of the bubble size on DO increase in the simulated experiment is shown in fig. 6, for the first 100 minutes after the start of electrolysis. A significant difference between simulations can be observed. All three computations are conducted with the same mass transfer coefficient. In reality, the difference is probably less pronounced than shown here, due to the increase of the mass transfer coefficient with increase of bubble diameter.

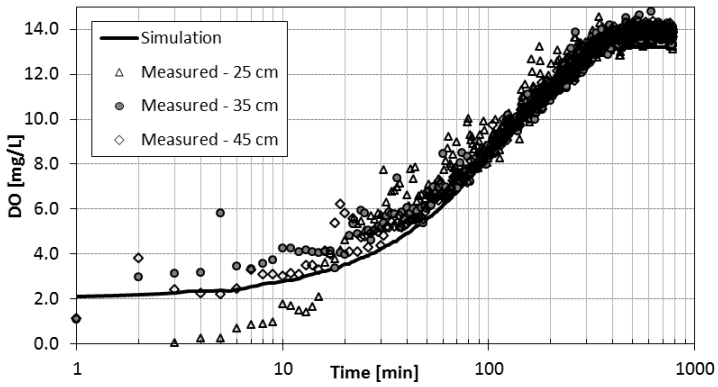

Figure 5. Comparison of simulated and calculated DO values: a) at 25cm, b) at 35cm, and c) at 45cm, from the bottom center.

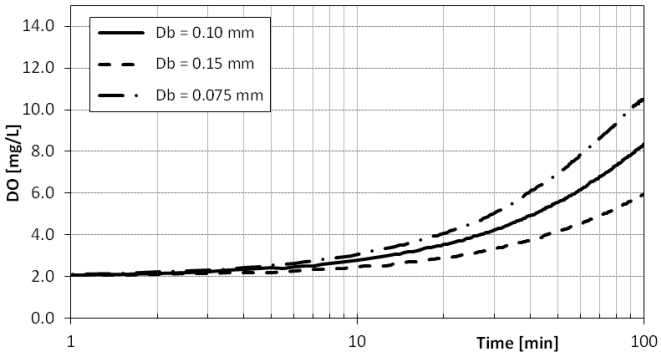

Figure 6. Simulation of DO increase at 25cm from the bottom center, as a function of the size of released oxygen bubbles

Simulation of the electrolysis field experiment

The simulated flow domain is the box itself and surrounding water, 60 cm around the box in the horizontal directions and the water column above the box up to the water surface (9 m). The molar volume of oxygen, at this pressure, is taken as 11.2 L/mol. Starting bubble diameter, as well as mass transfer coefficient is taken the same as in the simulation of the laboratory experiment. However, the Henry's constant is multiplied by 2, since 10m of water column represents approximately an additional atmosphere of pressure. The initial DO concentration in the whole domain was imposed as 0.4 mg/L. The experimental box is discretized by rectangular cells varying in size, from 2 × 2 × 2 cm near the walls, up to 6 × 6 × 6 cm.

The experiment is utilized to compare the standard k-ε turbulence model with the here presented the non-linear k-ε model. The non-linear k-ε models are attractive for the computations of flows influenced by anisotropy of the turbulence [34]. Therefore, it was interesting to analyze the difference in the case of the weak bubble plume flow, as in the case of electrolysis experiments presented here. The same mesh, boundary and initial conditions were applied for both calculations.

Calculated DO concentrations, at the location of the measurement probe, during the experiment are shown in Figure 7. The numerical model revealed the circulation flow pattern similar as in the laboratory experiment, which produces relatively uniform DO distribution, with slightly higher concentrations above the electrolysis plates and near the side walls of the box. It can be seen that DO concentrations increase approximately linearly and that both models reproduce the dynamics relatively well. Unfortunately, the experiment did not last enough to reach the limit value of DO concentration.

The linear k-ε model produced slightly higher concentrations throughout the simulation time in comparison with the non-linear one. The fig. 8 compares calculated turbulent kinetic energy at the middle profile, at the level of the probe and at the two time sections. It is expected to obtain the highest values in the region of strongest changes in liquid velocities [32]. While the distribution of the kinetic energy of turbulence is very similar, the non-linear k-ε model produced higher values of the eddy viscosity, with the difference reaching the 50%.

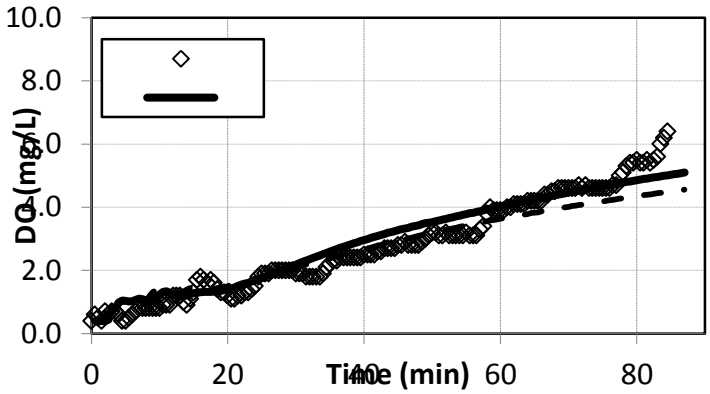

Figure 7. Comparison of measured and calculated DO concentrations at the location of the probe during the experiment.

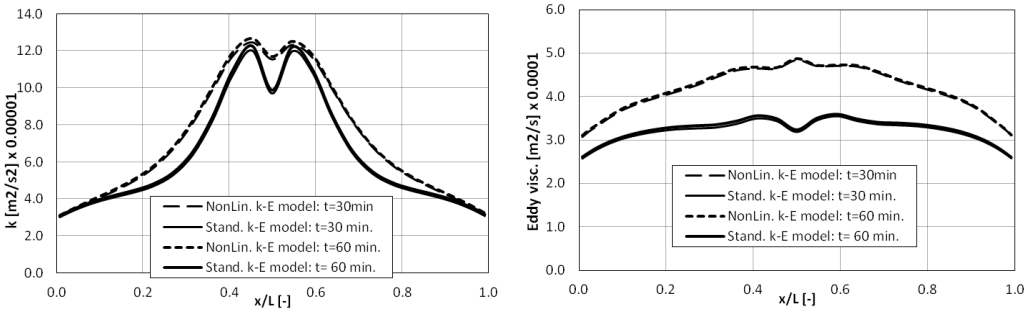

Figure 8. Comparison of the standard and the non-linear *k*-ε model results (Left: turbulence kinetic energy horizontal profiles at the level of the DO probe, Right: Eddy viscosity at the same profiles). The length is presented as nondimensional, by dividing the distance from the vertical wall with the box length.

Conclusions

In this paper we propose electrolysis as a novel hypolimnetic oxygenation tool. Due to the small bubble diameter produced, it showed to be very effective regarding dissolution of oxygen. If combined with hydrogen harvesting for energy purposes, it may even be economically viable. However, its applicability requires further experimental and modeling work to be done. In that respect, a three-dimensional numerical model for simulation of bubble plumes for DO recovery has been developed. Model is validated by simulation of bubble plume experiments reported in the literature, as well as on conducted electrolysis experiments.

Considering natural complexity of simulated processes and a number of adopted approximations in mathematical description, it can be concluded that developed model reproduced experiments of DO recovery reasonably well. The model experiments revealed significant sensitivity of DO recovery efficiency to initial bubble size. Therefore, additional research efforts are required to determine the initial bubble size of electrolysis and possible influence of physicochemical conditions. In regard of utilized turbulence model, it can be concluded that both models produced the similar DO concentration dynamics.

Acknowledgment

The research work is funded by Ministry of Education, Science, and Technological Development of Republic of Serbia through Technological Development Project no. TR 37009.

References

[1] Wetzel, R., G., *Limnology*, W. B. Saunders Company, Philadephia, USA, 1975
[2] Codd, G.A., Cyanobacterial toxins, the perception of water quality, and the prioritisation of eutrophication control, *Ecological Engineering*, 1 (2000), pp.51-60
[3] Cao, H.S., et al., Eutrophication and algal blooms in channe type reservois: a novel enclosure experiment by changing light intensity, *J. Environ. Sci. 23* (2011), 10, pp. 1660-1670
[4] Elci, S., Effects of thermal stratification and mixing on reservoir water quality, *Limnology*, *9* (2008), pp. 135-142
[5] Rangel-Peraza, J., et al., Modeling approach for characterizing thermal stratification and assessing water quality for a large tropical reservoir, *Lakes & Reservoirs: Research & Management, 17* (2012), 2, pp. 119-129
[6] Ma, W.X., et al., Study of the application of the water-lifting aerators to improve the water quality of a stratified, eutrophicated reservoir, *Ecological Engineering, 83* (2015), pp. 281-290
[7] Jones, R.A. and Lee G.F, Recent advances in assessing impact of phosphorus loads on eutrophication-related water quality, *Water Research, 16 (1982)*, 5, pp. 503-515
[8] Smith, V.H., et al., Eutrophication: impact of excess nutrient inputs on freshwater, marine, nd terrestrial ecosystems, *Environmental Pollution, 100* (1999), 1-3, pp. 179-196
[9] Sylvan, J.B., et al., Eutrophication-induced phosphorus limitation in the Mississippi River plume: Evidence from fast repetition rate fluorometry, *Limnology and Oceanography. 56* (2007), 6, pp. 2679-2685
[10] McGinnis, D.F. and Little, J.C., Predicting diffused-bubble oxygen transfer rate using the discrete-bubble model, *Water Research, 36* (2002), pp. 4627-4635
[11] Beutel, M.W. et al., Effects of aerobic and anaerobic condidtions on P, N, Fe, Mn and Hg accumulation in waters overlaying prundal sediments of an oligo-mesotrophic lake, *Water Research, 42* (2008), pp. 1953-1962
[12] Bryant, L.D., et al., Solving the problem at the source: Controlling Mn releaseat the sediment-water interface via hypolimentic oxygenation, *Water Resources, 45* (2011), pp.6381-6392
[13] Little, J.C., Hypolimnetic aerators: Predicting oxygen transfer and hydrodynamics, *Water Research, 29* (1995), 11, pp.2475-2482
[14] Janczak, J. and Kowalik, A., Assessment of the efficiency of artificial aeration in the restoration of Lake Goplo, *Limnological Review, 1* (2001), pp. 151-159
[15] McGinnis, D.F., et al., Interaction between a bubble plume and the near field in a stratified lake, *Water Resources Research, 40* (2004), W10206
[16] Gafsi, M., et al., Comparative studies of the different mechanical oxygenation systems used in the restoration of lakes and reservoirs, *J. of Food, Agricalture & Environment, 7* (2009), (2), pp. 815-822
[17] Schladow, S. G., Bubble Plume Dynamics in a Stratified Medium and the Implications for Water Quality Amelioration in Lakes, *Water Resour. Res. 28* (1992), 2, pp. 313-321
[18] Wuest, A., et al., Bubble Plume Modeling for Lake Restoration, *Water Resour. Res. 28* (1992.), 12, pp. 3235-3250
[19] Sahoo, G.B. and Luketina, D., Modeling of bubble plume design and oxygen transfer for reservoir restoration, *Water Research 37* (2003), pp. 393-401
[20] Aseada, T. and J. Imberger, Structure of bubble plumes in linearly stratified environments, J. Fluid Mech., 249 (1993), pp. 35-57
[21] Lemckert, Ch. and J. Imberger, Energetic bubble plumes in arbitrary stratification, *J. Hydraul. Eng., 119* (1993), pp. 680-703
[22] Bernard, R.S., et al., A simple computational mode for bubble plues, *Applied Mathematical Modelling, 24* (2000), pp. 215-233
[23] Sokolichin, A. and Eigenberger, G., Gas-liquid flow in bubble columns and loop reactors: Part I. Detailed modelling and numerical simulation, *Chem. Eng. Sci., 49* (1994), 24B, pp. 5735-5746

[24] Becker. S., et al., Gas-liquid flow in bubble columns and loop reactors: Part II. Comparison of detailed experiments and flow simulations, *Chem. Eng. Sci., 49* (1994), 24B, pp. 5747-5762
[25] Buscaglia, G.C., et al., Numerical modeling of large-scale bubble plumes accounting for mass transfer effects, *Int. J. of Multiphase Flow, 28* (2002), pp.1763-1785
[26] Fraga, B., et al., A LES-based Eulerian-Lagrangian approach to predict the dynamics of bubble plumes, *Ocean modelling, 97* (2016), pp. 27-36
[27] Hirt, C.W. and Nichols, B.D., Volume-of-fluid (VOF) method for the dynamics of free boundaries, *J. Comput. Phys., 39* (1981), pp. 201-225
[28] Sokolichin, A., et al., Dynamic numerical simulation of gas-liquid two-phase flows Euler/Euler vs Euler/Lagrange, *Chem Eng. Sci., 52* (1997), 4, pp.611-626
[29] Hassanizadeh, M. and W.G. Gray, General conservation equations for multiphase systems: 1. Averaging procedure, *Adv. Water Res., 2* (1979), pp. 131-144
[30] Tomiyama, A., et al., Drag coefficients of single bubbles under normal and micro gravity conditions, *JSME Int. J. Series, B41* (1998), pp. 472-479
[31] Hirt, C.W. and Cook, J.L., Calculating Three-Dimensional Flows around Structures and over Rough Terrain, *Jour. Comp. Phys., 10* (1972), 324-340
[32] Hirsch, C., Numerical computation of internal and external flows, Vol. 2: Computational methods for inviscid and viscous flows, J. Willey & Sons., (1990)
[33] Sokolichin, A. and Eigenberger, G., Applicability of the standard *k*-ε turbulence model to the dynamic simulation of bubble columns. Part I: Detailed numerical simulation, *Chem. Eng. Sci., 54* (1999), pp. 2273-2284
[34] Dhotre, M.T., et al., Large eddy simulation for dispersed bubbly flows: a review, *Int. J. Chem. Eng., 2013* (2013), pp.1-22
[35] Kimura, I. and Hosoda, T., A non linear k- model with realizability for prediction of flows around bluff bodies, *Int. J. Numer. Meth. Fluids, 42* (2003), pp. 813-837
[36] Jacimovic, N. et al., Numerical modeling of dissolved oxygen recovery during aeration in lakes, Proceedings of the 6th International Symposium on Environmental Hydraulics (6th ISEH), Vol. 2 (2010), pp. 729-734.
[37] Borchers, O., et al., Applicability of the standard *k*-ε turbulence model to the dynamic simulation of bubble columns. Part II: Comparison of detailed experiments and flow simulations, *Chem. Eng. Sci., 54* (1999)., pp. 5927-5735

Paper submitted: February 1, 2016
Paper revised: May 30, 2016
Paper accepted: July 14, 2016